

A HIGH-METALLICITY HIGH VELOCITY CLOUD ALONG THE MRK 421 SIGHT LINE: A TRACER OF COMPLEX M?

YANGSEN YAO¹, J. MICHAEL SHULL¹, AND CHARLES W. DANFORTH¹

Accepted for publication in the *Astrophysical Journal Letters*

ABSTRACT

We present a new measurement, $0.85 - 3.5Z_{\odot}$, of the metallicity of high velocity cloud (HVC) Complex M by analyzing ultraviolet spectroscopic observations of the blazar Mrk 421 taken with the Cosmic Origins Spectrograph on the *Hubble Space Telescope* and the *Far Ultraviolet Spectroscopic Explorer*. Although an HVC at $V_{\text{LSR}} = -131 \text{ km s}^{-1}$ is not visible in 21 cm emission ($\log N_{\text{HI}} < 18.38; 3\sigma$), it is detected in ultraviolet absorption lines of C II, N I, O I, O VI, Si II, Si III, Si IV, Fe II, and H I. By referencing velocities to the intermediate velocity cloud at -60 km s^{-1} and jointly analyzing H I absorption from high-order H I Lyman lines, we measure $\log N_{\text{HI}} = 16.84^{+0.34}_{-0.13}$ (1σ) in the HVC. Comparing H I and O I, we find an HVC metallicity $[\text{O}/\text{H}] = 0.32^{+0.22}_{-0.39}$. Because the sight line passes $\sim 4^{\circ}$ from the HVCs in Complex M, the detected HVC may represent the highest velocity component of the Complex, and our measurements provide a lower limit to its metallicity. The high, possibly super-solar metallicity, together with the low distance, $z < 3.5 \text{ kpc}$, above the Galactic plane suggest that Complex M is condensed returning gas from a Galactic fountain.

Subject headings: ISM: clouds — ISM: abundances — ISM: structure — ultraviolet: ISM

1. INTRODUCTION

The gaseous clouds surrounding the Milky Way are observed at near-zero velocity, as well as in intermediate velocity clouds (IVCs) and high velocity clouds (HVCs). The latter are defined as interstellar gas with absolute velocities relative to the local standard of rest (LSR) between $|V_{\text{LSR}}| = 30 - 90 \text{ km s}^{-1}$ and $|V_{\text{LSR}}| > 90 \text{ km s}^{-1}$, respectively. These clouds are inconsistent with the simple model of Galactic rotation (see review by Wakker 2001). The IVCs and HVCs are detected not only in neutral and mildly ionized species like H I, C II, O I, S II, and Si II (Murphy et al. 1995; Wakker & van Woerden 1997; Collins et al. 2003) but also in highly ionized species like C IV, O VI, N V, and Si IV (Sembach et al. 2003; Collins et al. 2004; Fox et al. 2006; Lehner & Howk 2010).

The IVCs have near-solar metal abundances, are found within several kpc of the Galactic plane (e.g., Wakker et al. 1996; Ryans et al. 1997; Richter et al. 2001), and are consistent with the Galactic fountain interpretation. However, the origin of HVCs is still poorly understood. The proposed scenarios include the Galactic fountain (Shapiro & Field 1976; Houck & Bregman 1990), cooling Galactic halo gas falling onto the Galactic plane (Wakker et al. 1999; Collins et al. 2003; Shull et al. 2009), warm-hot intergalactic medium (WHIM) in the Local Group (Blitz et al. 1999; Braun & Burton 1999), and combinations of all three (Tripp et al. 2003). These competing models predict distinct scale sizes and metallicities of HVCs, ranging from several kpc with near-solar abundances (fountain model), to tens of kpc with subsolar abundances (halo model), to hundreds of kpc with primordial abundances (the WHIM model). Clearly, distances and metallicities are key measurements for constraining the origin of HVCs.

The HVC Complex M lies at the highest Galactic latitude

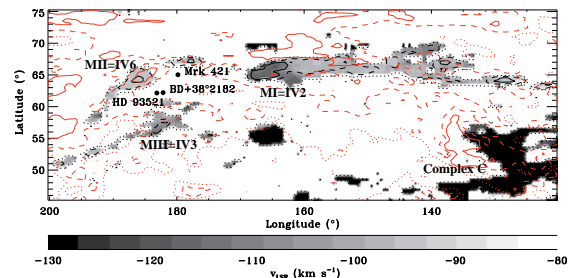


FIG. 1.— 21 cm emission observations toward Complex M region. Grey-scale image shows HVC in range $V_{\text{LSR}} = -80$ to -130 km s^{-1} . Black contours indicate brightness levels 0.2, 0.5, and 1 K, and red contours indicate IVCs with brightness levels 0.5, 1, and 2 K. Three sight lines of interest and core regions of M I, M II, M III and their corresponding IVCs are also marked. Figure is similar to Figure 5 of Wakker (2001) but using observations of LAB H I survey.

among known HVC complexes, covering $b = 45^{\circ}$ to 70° and longitudes from $\ell = 130^{\circ}$ to 200° , over a velocity range of $-125 < V_{\text{LSR}} < -85 \text{ km s}^{-1}$ (Hulsbosch 1968). It is composed of several distinct HVC clouds (M I, M II, and M III) that are apparently superposed with several intermediate velocity clouds in the sky, including the IV Arch (IV2, IV6, and IV3; Fig. 1; Giovanelli et al. 1973; Wakker & van Woerden 1991; Kuntz & Danly 1996). In a comparison of spectroscopic observations of two Galactic halo stars HD 93521 and BD+38°2182 (Fig. 1) observed with the *International Ultraviolet Explorer* (IUE), Danly et al. (1993) found high velocity wings at $V_{\text{LSR}} < -85 \text{ km s}^{-1}$ in O I, Si III, and C II absorption in spectra of BD+38°2182 ($z \approx 4.4 \text{ kpc}$) but not in HD 93521 ($z \approx 1.5 \text{ kpc}$). They estimated the distance of Complex M (M II and M III) to lie between $1.5 < z < 4.4 \text{ kpc}$ above the Galactic plane. Ryans et al. (1997) made further differential optical observations of stars in the region and revised the distance ($z = 3.5 \text{ kpc}$) to BD+38°2182. They argued that the absence of high-velocity absorption along the HD 93521 sight line could be due to small-scale spatial variation of the Complex, and suggested decreasing the lower limit to its distance.

The metallicity of Complex M is much less certain. Combining a much deeper 21-cm emission limit, $\log N_{\text{HI}} < 17.43$

¹ Center for Astrophysics and Space Astronomy, Department of Astrophysical and Planetary Sciences, University of Colorado, 389 UCB, Boulder, CO 80309; yaoy@colorado.edu, michael.shull@colorado.edu, charles.danforth@colorado.edu

from the Jodrell Bank 76m, with O I absorption measurements by Danly et al. (1993) along the BD+38°2182 sight line, Ryans et al. (1997) estimated an oxygen abundance $> 0.5Z_{\odot}$ for the MIII cloud. Wakker (2001) constrained the metallicity of the MI cloud to be 0.4–1.8 Z_{\odot} based on S II and H I emission data in the core region of MI; the large range arises from uncertainty in the ionization correction. Because of its short distance and possible high metallicity, Complex M is believed to be part of the IV Arch (Kuntz & Danly 1996; Wakker 2001).

In this *Letter*, we analyze an HVC along the sight line to the blazar Mrk 421 and set a tight lower limit to the metallicity of Complex M. Savage et al. (2005) detected the HVC in H I, C II, and C III absorption lines in the *FUSE* spectrum, but they focused on the origin of the extended red wing of O VI absorption. Throughout, we quote errors at 1σ and upper limits at 3σ confidence levels. We adopt atomic data from Morton (2003) and solar abundances from Asplund et al. (2009), in particular, $\log(X/H)_{\odot} + 12 = 8.43, 7.83, 8.69, 7.51, 7.12$, and 7.50 for C, N, O, Si, S, and Fe, respectively.

2. OBSERVATIONS AND DATA REDUCTION

Our data come from far ultraviolet spectroscopic observations of the background target Mrk 421 ($l, b = 179.83^{\circ}, 65.03^{\circ}$; $z = 0.03$) obtained with the Cosmic Origins Spectrograph (COS; Osterman et al. 2011) aboard the *Hubble Space Telescope (HST)* and with the *Far Ultraviolet Spectroscopic Explorer (FUSE)*. Mrk 421 is one of the Guaranteed Time Observation (GTO; PI: Green) targets of COS, which has two medium-resolution gratings G130M and G160M, covering wavelengths 1150–1450 Å and 1405–1775 Å with a spectral resolution $\sim 18,000$. The *FUSE* data cover 905–1187 Å with a resolution $\sim 20,000$. COS observed Mrk 421 on 2009 November 24 (PID 11520) with total exposures of 1.7 ks (G130M) and 1.8 ks (G160M). *FUSE* observed the source on 2000 December 1 (PID P101) and 2003 January 19 (PID Z010) with a total exposure of 85.0 ks.

The observations and calibrated data were retrieved from the Multimission Archive (MAST²) at the Space Telescope Science Institute. The COS data were further processed following the procedure described in Danforth et al. (2010). Only the *FUSE* LiF1a and SiC2a data were used, reduced further as described in Danforth et al. (2006). Individual exposures were weighted by their exposures and coadded to form final spectra, whose signal-to-noise ratios per resolution element range from 25–35 (COS) and 5–15 (*FUSE*). We find $< 5\%$ flux fluctuation in the COS spectra arising from unremoved small fixed-pattern features. These fluctuations, compared to systematic uncertainties in wavelength calibration, are not important in measurements described below.

The wavelengths of these spectra were calibrated with respect to the H I 21 cm emission data from Leiden/Argentine/Bonn (LAB), which have an angular resolution of $\sim 0.6^{\circ}$, spectral resolution of 1.3 km s^{-1} , and rms brightness-temperature noise of 70–90 mK (Kalberla et al. 2005). Four LAB pencil beams adjacent to the Mrk 421 sight line were extracted, averaged, and weighted by the inverse square of their angular separations from the sight line. An IVC component is clearly resolved from the zero-velocity component in the final emission spectrum. We use a Gaussian fit to the IVC and obtain its LSR velocity, column density, and

TABLE 1
HVC MEASUREMENT

ions	b (km s^{-1})	$\log N$ (N in cm^{-2})
Si II	13.9 ± 1.1	13.05 ± 0.02
Si IV	16.2 ± 4.0	12.55 ± 0.08
Fe II	(0, 13.9)	13.31 ± 0.15
S II	13.9(fixed)	< 13.37
C II	12.7 ± 1.5	13.91 ± 0.03
C IV	13.9(fixed)	< 12.55
N I	13.9(fixed)	12.79 ± 0.12
N V	13.9(fixed)	< 12.53
O VI	(6.9, 14.5)	13.01 ± 0.16
O I	10.7 ± 3.8	13.85 ± 0.05
H I	13.9(fixed)	$16.84^{+0.34}_{-0.13}$

NOTE. — b is Doppler width of the absorption line, and N is the ionic column density. Uncertainties are statistical except for N_{HI} , which includes wavelength calibration uncertainties of *FUSE* observations. See text for details.

Doppler width: $v_{\text{HI}}^{(\text{IVC})} = -60 \text{ km s}^{-1}$, $N_{\text{HI}}^{(\text{IVC})} = 6.82 \times 10^{19} \text{ cm}^{-2}$, and $b_{\text{HI}}^{(\text{IVC})} = \sqrt{2}\sigma = 17.5 \text{ km s}^{-1}$ (Fig. 2a). The IVC can also be resolved in lines of S II $\lambda 1259.529$ (COS), Si II $\lambda 1020.699$ (*FUSE* LiF1a), and O I $\lambda 929.517$ (*FUSE* SiC2a) – see Figs. 2 and 3. We shift the ultraviolet spectra to align their IVC velocities with the 21 cm data.

In the shifted spectra, an HVC at -131 km s^{-1} is visible in Si II, O I, N I, and C II at $> 3\sigma$ significance, and in Si IV, O VI, and Fe II at 2–3 σ significance. All line centroids are well aligned within $\sim 15 \text{ km s}^{-1}$ (Figs. 2 and 3). The HVC, however, is not visible in the 21 cm data (Fig. 2a).

3. HVC MEASUREMENT AND RESULTS

We use the model developed in Yao et al. (2010) to measure absorption of the HVC. This model uses ionic column density (N) and Doppler width (b_D) as fitting parameters and adopts a Voigt function to approximate the absorption-line profile. This model can be used to fit individual absorption lines or to jointly analyze multiple absorption lines. We include instrumental line spread functions (LSFs) in our spectral fit by using the wavelength-dependent LSF of COS observations³ and a Gaussian with FWHM 20 km s^{-1} across the entire wavelength range of *FUSE* observations. Because Si II has multiple transitions (Fig. 2), we jointly analyze these lines to reduce statistical uncertainty. This method is equivalent to a curve-of-growth analysis but propagates errors automatically. The consistent Doppler widths measured in Si II and O I (11 – 14 km s^{-1}) indicate that non-thermal broadening dominates the line width. To measure column densities or upper limits for ions whose HVC components are unresolved or whose line widths are unconstrained, we fix their line centroids and their widths to those of Si II. Our results are presented in Table 1. Because Si III and C III in the HVC are severely blended with the IVC components, we have not measured their column densities.

We are able to measure N_{HI} in the high Lyman lines of the HVC by subtracting out H I absorption from the IVC and low-velocity gas. Both components are saturated, but only the IVC (-60 km s^{-1}) contributes to the absorption in higher Lyman lines at the (-131 km s^{-1}) velocity of the HVC (Fig. 3). Since we have well-determined values of $v_{\text{HI}}^{(\text{IVC})}$, $b_{\text{HI}}^{(\text{IVC})}$, and $N_{\text{HI}}^{(\text{IVC})}$ from 21 cm data (§ 2), we fix its absorption in the

² <http://archive.stsci.edu/>

³ http://www.stsci.edu/hst/cos/performance/spectral_resolution/

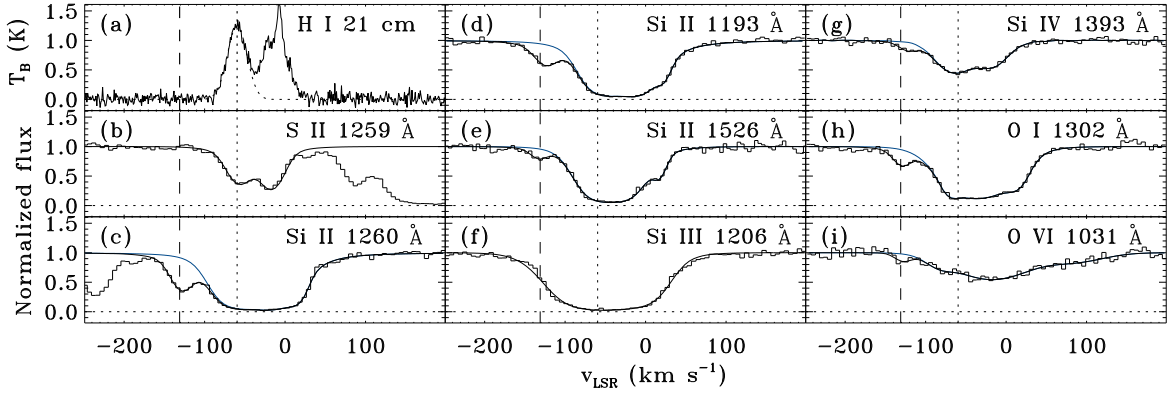


FIG. 2.— LAB 21-cm emission data and UV absorption lines observed along Mrk 421 sight line. Thick black curves are the spectral fit, and blue curves indicate local “continuum” of HVC absorption. Vertical dotted and dashed lines indicate centroids of IVC and HVC at -60 km s^{-1} and -131 km s^{-1} , respectively. See text for details.

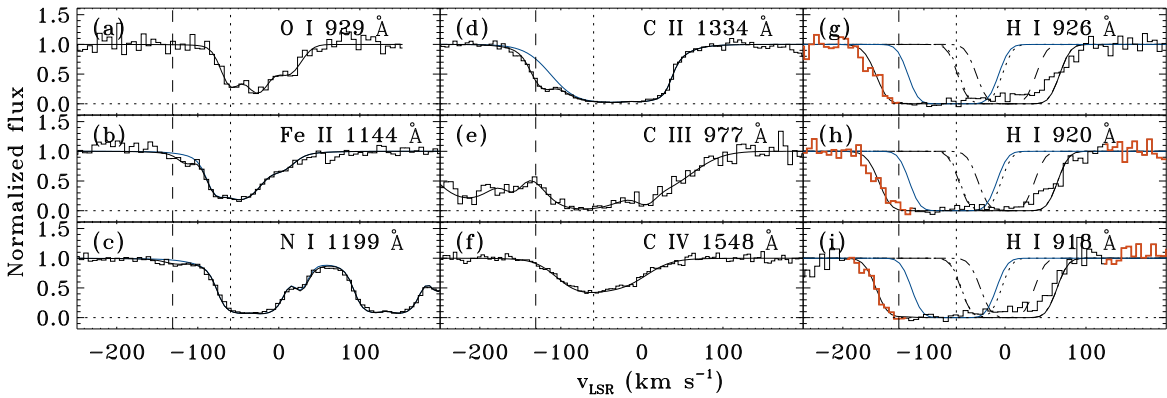


FIG. 3.— Same as Fig. 2. In panels g-i, data marked with red are spectral ranges used in constraining the HVC H I absorption, and the solid blue, dotted, dashed, and dot-dashed curves indicate absorption of the four emission components at -60 , -28 , -8 , and $+18 \text{ km s}^{-1}$ revealed in the Green Bank data (Savage et al. 2005). $\text{Ly}\eta$ to $\text{Ly}\lambda$ are used in our spectral analysis, but only three Lyman lines are plotted for demonstration. See text for details.

total H I spectrum and fit the remaining absorption as the HVC contribution. The deuterium (D I) absorption lines lie -82 km s^{-1} blueward of the corresponding H I lines. Thus, D I in the IVC lies at -142 km s^{-1} and gives a small amount of contamination to the HVC H I absorption at -131 km s^{-1} . We model the D I absorption by adopting the abundance in the local ISM, $(\text{D}/\text{H}) = 1.6 \times 10^{-5}$ (Linsky et al. 1993) and assuming that thermal broadening dominates its line width, $b_{\text{DI}}^{(\text{IVC})} = b_{\text{HI}}^{(\text{IVC})}/\sqrt{2}$. To minimize the uncertainties caused by line saturation, we only use blue-rising wings of five high-order transitions of H I, from $\text{Ly}\eta$ to $\text{Ly}\lambda$ (Fig. 3). We jointly fit these five H I lines to reduce statistical uncertainties, allowing their positions to vary by $\pm 10 \text{ km s}^{-1}$ around the expected HVC velocity to account for possible systematic wavelength drift. In the joint fit, we set $b_{\text{HI}}^{(\text{HVC})} = b_{\text{SiII}}^{(\text{HVC})}$. The resulting column density, $\log N_{\text{HI}}^{(\text{HVC})} = 16.84^{+0.34}_{-0.13}$ (Table 1) is much better determined than the upper limit found from the 21 cm data, $\log N_{\text{HI}}^{(\text{HVC})} < 18.38$ (3σ), integrated over a velocity range of 23 km s^{-1} , the FWHM of the Si II absorption line (Table 1).

4. DISCUSSION AND SUMMARY

The Mrk 421 sight line probes an interesting region of HVC Complex M. It lies approximately 4° away from the MI, MII, and MIII clouds and passes through the IVC IV26 (Fig. 1; see also Fig. 1 in Savage et al. 2005 and Fig. 5 in Wakker 2001). An apparent (LSR) velocity change from -112 km s^{-1} at $l = 170^\circ$ to -117 km s^{-1} at $l = 160^\circ$ was observed in pre-

vious studies of MI (Wakker & van Woerden 1991). The detected velocity (-130 km s^{-1}) along the Mrk 421 sight line is inconsistent with this trend, but it fits into a larger scale ($\gtrsim 20^\circ$) picture in which the velocities of MI increase toward higher longitudes and lower latitudes, connecting with MIII whose velocities increase toward lower longitudes and higher latitudes (Fig. 1; also see Fig. 5 in Wakker 2001). Thus, the sight line likely probes the high velocity end of Complex M.

The HVC along the Mrk 421 sight line has been suggested in H I, C II, and C III absorption lines in the *FUSE* spectrum. Savage et al. (2005) measured a surprisingly large value, $N_{\text{HI}}^{(\text{HVC})} = 4.8^{+6.9}_{-2.8} \times 10^{18} \text{ cm}^{-2}$ ($\log N_{\text{HI}} = 18.68 \pm 0.38$) in a component fit to the saturated H I Lyman lines $\text{Ly}\beta$ – $\text{Ly}\delta$, nearly 70 times higher than that (Table 1) obtained in this work. To examine possible causes of this discrepancy, we superpose the amount of the four velocity components revealed from the Green Bank observation (Savage et al. 2005) on the H I absorption spectra (Fig. 3g-i). Clearly, only the blue wing of the IVC at -60 km s^{-1} affects the $N_{\text{HI}}^{(\text{HVC})}$ determination. To further examine possible effects of beam smearing, we extracted the LAB emission data within 1° around the Mrk 421 sight line. Unlike the other three emission components, whose brightness temperatures can vary by a factor of five, $N_{\text{HI}}^{(\text{IVC})}$ increases smoothly toward large longitudes and high latitudes, with fluctuations $\Delta N_{\text{HI}}^{(\text{IVC})}/N_{\text{HI}}^{(\text{IVC})} \lesssim 10\%$ among the four beams closest to the Mrk 421 sight line. Taking this variation into account in our analysis, we find that

the change in $N_{\text{HI}}^{(\text{HVC})}$ is negligible compared to that caused by the systematic uncertainty of the wavelength calibration. We conclude that our result is not affected by beam smearing, although we cannot completely rule out variations of the IVC absorption on angular scales < 10 arcmin, which could significantly change our results. We speculate that the apparently large $N_{\text{HI}}^{(\text{HVC})}$ obtained by Savage et al. (2005) is caused by the severely underestimated $N_{\text{HI}}^{(\text{IVC})}$ in their fit.

The measured $N_{\text{OI}}^{(\text{HVC})}$ and $N_{\text{HI}}^{(\text{HVC})}$ give a metallicity in the HVC along the Mrk 421 sight line of $[\text{O}/\text{H}] = 0.32^{+0.22}_{-0.39}$ or $0.85\text{--}3.5 Z_{\odot}$. The large uncertainty is caused by systematic uncertainty in the wavelength calibration introduced in our joint analysis of the H I Lyman series (§ 3). Because O I and H I have nearly the same ionization potential and are coupled by resonant charge exchange, this measurement accurately reflects the gas-phase oxygen abundance and is not subject to ionization correction. In measuring $N_{\text{HI}}^{(\text{HVC})}$, we assumed $b_{\text{DI}}^{(\text{IVC})} = b_{\text{HI}}^{(\text{IVC})} / \sqrt{2}$ and $b_{\text{HI}}^{(\text{HVC})} = b_{\text{SiII}}^{(\text{HVC})}$ and adopted the local-ISM deuterium abundance, $(\text{D}/\text{H}) = 1.6 \times 10^{-5}$, one of the lowest interstellar abundances (Robert et al. 2000). Adopting higher values of for D/H or b_{DI} will result in a smaller $N_{\text{HI}}^{(\text{HVC})}$. Therefore the inferred oxygen abundance should be regarded as a conservative lower limit. Ionization corrections need to be applied in calculating the abundances of Si, S, or Fe. For a photoionized plasma with hydrogen number density $n_{\text{H}} = 0.1 \text{ cm}^{-3}$ and $\log N_{\text{HI}} \leq 17.5$, the (logarithmic) ionization corrections are 1.30, 1.42, and 0.90 for Si II, S II, and Fe II, respectively (Mark Giroux, private communication, 2010). Taking the best-fit values (Table 1), we obtain $[\text{X}/\text{H}] = -0.6, < 0.22, \text{ and } 0.07$ for Si, S, and Fe. Owing to the unconstrained n_{H} , the systematic uncertainty could be high in the inferred $[\text{Si}/\text{H}]$, $[\text{S}/\text{H}]$, and $[\text{Fe}/\text{H}]$. However, this exercise results in consistently high metal abundances, except for a slightly lower value for Si. Within uncertainties, the high metallicity is consistent with values $0.4\text{--}1.8 Z_{\odot}$ in MI (Wakker 2001), $> 0.5 Z_{\odot}$ in MIII (Ryans et al. 1997), and the near-solar metallicity of IV3 (Spitzer & Fitzpatrick 1993). The consistency also suggests that the HVC toward Mrk 421 is associated with Complex M and the lower velocity IV Arch.

The measured oxygen abundance provides a new lower limit to the metallicity of Complex M.

The high metallicity, together with the upper limit on distance of other parts of Complex M, shed light on its origin. Unlike the highly ionized HVCs, in which the high ions (O VI and C IV) are significant or even dominant, the HVC toward Mrk 421 is dominated by low ions (O I, C II, S II; Table 1). This suggests distinct ionization conditions of this HVC compared to the highly ionized, low H I column density HVCs (Sembach et al. 2003; Collins et al. 2004, 2005; Fox et al. 2006; Lehner & Howk 2010). Such mildly ionized, low H I column density HVCs have recently been surveyed by several groups (e.g., Richter et al. 2009; Shull et al. 2009; Collins et al. 2009). Richter et al. (2009) also provided ionization modeling for the HVCs with different distances. Substituting $N_{\text{OI}}^{(\text{HVC})}$ and $N_{\text{SiII}}^{(\text{HVC})}$ (Table 1) into their model and assuming no depletion of Si into dust grains, we obtain a gas density $n_{\text{H}} = 3.4 \text{ cm}^{-3}$ and absorption path length $L = 0.007\text{--}0.02$ pc for Complex M. The near-solar (likely supersolar) abundance, short path length, and large gas density clearly rule out the WHIM model and disfavor the halo model (§ 1) for the HVC. Complex M likely traces a supernova shell that has not been ejected too far above the Galactic plane and is now falling back to the Galactic disk.

In summary, we have presented an interstellar high velocity cloud detected in ultraviolet spectroscopic observations of Mrk 421, which represents the highest velocity end of the HVC Complex M. The combination of *HST*-COS and *FUSE* observations enables us to obtain a lower limit, $> 0.85 Z_{\odot}$, to the metallicity of the Complex. The high metallicity and the short distance are consistent with Complex M being the returning gas of a Galactic fountain.

The authors have benefited from the discussions with Nicolas Lehner and comments from an anonymous referee. This work at the University of Colorado was partly supported by NASA grant NNX08AC14G for data analysis and scientific discoveries related to the Cosmic Origins Spectrograph on the Hubble Space Telescope, and by NNX07AG77G for theoretical work (JMS). YY also appreciates financial support by NASA through ADP grant NNX10AE86G.

REFERENCES

- Asplund, M., Grevesse, N., Sauval, A., & Scott, P. 2009, *ARA&A*, 47, 481
 Blitz, L., Spergel, D. N., Teuben, P. J., Hartmann, D., & Burton, W. B. 1999, *ApJ*, 514, 818
 Braun, R., & Burton, W. B., 1999, *A&A*, 341, 437
 Collins, J. A., Shull, J. M., & Giroux, M. L. 2003, *ApJ*, 585, 336
 Collins, J. A., Shull, J. M., & Giroux, M. L. 2004, *ApJ*, 605, 216
 Collins, J. A., Shull, J. M., & Giroux, M. L. 2005, *ApJ*, 623, 196
 Collins, J. A., Shull, J. M., & Giroux, M. L. 2009, *ApJ*, 705, 962
 Danforth, C. W., Shull, J. M., Rosenberg, J. L., & Stocke, J. T., 2006, *ApJ*, 640, 716
 Danforth, C. W., Keeney, B. A., Stocke, J. T., Shull, J. M., & Yao, Y. 2010, *ApJ*, 720, 976
 Danly, L., Albert, C. E., & Kuntz, K. D. 1993, *ApJ*, 416, L29
 Fox, A. J., Savage, B. D., & Wakker, B. P. 2006, *ApJS*, 165, 229
 Giovanelli, R., Verschuur, G. L., & Cram, T. R. 1973, *A&AS*, 12, 209
 Houck, J. C., & Bregman, J. N. 1990, *ApJ*, 352, 506
 Hulsbosch, A. N. M. 1968, *Bull. Astron. Inst. Netherlands*, 20, 33
 Kalberla, P. M. W., Burton, W. B., Hartmann, D., Arnal, E. M., Bajaja, E., Morras, R., & Pöppel, W. G. L. 2005, *A&A*, 440, 775
 Kuntz, K. D., & Danly, L. 1996, *ApJ*, 457, 703
 Lehner, N., & Howk, J. C. 2010, *ApJ*, 709, L138
 Linsky, J. L., et al. 1993, *ApJ*, 402, 694
 Morton, D. 2003, *ApJS*, 149, 205
 Murphy, E. M., Lockman, F. J., & Savage, B. D. 1995, *ApJ*, 447, 642
 Osterman, S., et al. 2011, *Ap&SS*, in press, astro-ph/1012.5827
 Richter, P., Sembach, K. R., Wakker, B. P., Savage, B. D., Tripp, T. M., Murphy, E. M., Kalberla, P. M. W., Jenkins, E. B. 2001, *ApJ*, 559, 318
 Richter, P., Charlton, J. C., Fangano, A. P., Bekhti, N. B., & Masiero, J. R. 2009, *ApJ*, 695, 1631
 Robert, F., Gautier, D., & Dubrulle, B. 2000, *Space Sci. Rev.*, 92, 201
 Ryans, R. S. I., Keenan, F. P., Sembach, K. R., & Davies, R. D. 1997, *MNRAS*, 289, 83
 Savage, B. D., Wakker, B. D., Fox, A. J., & Sembach, K. R. 2005, *ApJ*, 619, 863
 Sembach, K. R., et al. 2003, *ApJS*, 146, 165
 Shapiro, P. R., & Field, G. B. 1976, *ApJ*, 205, 762
 Shull, J. M., Jones, J. R., Danforth, C. W., & Collins, J. A. 2009, *ApJ*, 699, 754
 Spitzer, L., & Fitzpatrick, E. L. 1993, *ApJ*, 409, 299
 Tripp, T. M., et al. 2003, *AJ*, 125, 3122
 Wakker, B. P., & van Woerden, H. 1991, *A&A*, 250, 509
 Wakker, B. P., Howk, C., Schwarz, U., van Woerden, H., Beers, T., Wilhelm, R., Kalberla, P., & Danly, L. 1996, *ApJ*, 473, 834
 Wakker, B. P., & van Woerden, H. 1997, *ARA&A*, 35, 217
 Wakker, B. P., et al. 1999, *Nature*, 402, 388
 Wakker, B. P. 2001, *ApJS*, 136, 463
 Yao, Y., Shull, J. M., Danforth, D. W., Keeney, B. A., & Stocke, J. T. 2011, *ApJ*, in press